

# Chapter 36

## Integration of GNSS and Seismic Data for Earthquake Early Warning: A Case Study on the 2011 Mw 9.0 Tohoku-Oki Earthquake

Bofeng Guo, Xiaohong Zhang and Xingxing Li

**Abstract** Earthquake early warning (EEW), which is considered to be a pragmatic and viable way to reduce the damage and casualties during a large earthquake, relies on the accurate estimation of broadband displacements and the capability of rapidly detection of the first arrival wave (P-wave). Real-time high-rate GNSS is a reliable tool to directly capture displacements including static offsets and dynamic motions at the near field, which does not suffer from the clip, rotation and tilt problems as the traditional seismic instrument does. However, due to the large high-frequency noise and the low sampling rates of GNSS measurements, it is hard to pick up the P-wave arrival accurately in GNSS-derived displacement history. To overcome this problem, the combination of high-rate GNSS and collocated accelerometers shows promise as a more reliable and effective way, because accelerometers perform very well with high precision in the high-frequency range. In this study, we investigate the method by using collocated GNSS and accelerometers for EEW. We first introduce a new approach, namely the temporal point positioning (TPP) method, which could directly obtain coseismic displacement with a single GNSS receiver in real-time. The TPP method overcome the convergence problem of precise point positioning (PPP), and also avoids the integration process of the Variometric approach. And then we apply a multi-rate Kalman filter to fuse GNSS-derived coseismic displacement with collocated accelerometer data for attaining integrated displacements with a high precision and reliability. Finally, we detect the arrival time of P-wave and determine the earthquake magnitude from the integrated results. The performance of collocated GNSS and accelerometers is validated using data from GEONET (1 Hz GPS) and K-NET/KiK-Net (100 Hz accelerometer) stations, with the collocated distance less than 2 km, in the near field of the Mw 9.0

---

B. Guo (✉) · X. Zhang · X. Li

School of Geodesy and Geomatics, Wuhan University, 129 Luoyu Road, Wuhan 430079  
Hubei, China  
e-mail: guobofeng@whu.edu.cn

X. Li

German Research Centre for Geosciences (GFZ), Telegrafenberg 14473 Potsdam, Germany

Tohoku-Oki earthquake occurred on March 11, 2011. Using the broadband displacements derived by the above method, we detect the arrival time of P-wave with a mean value 0.15 s offset different from the USGS reference values, and the estimated magnitude is  $M_w$  9.06, which is achievable within 2–3 min after earthquake initiation.

**Keywords** Temporal point positioning · Earthquake early warning · Real-time high-rate GNSS · Accelerometer · Integrated displacement

## 36.1 Introduction

Earthquake early warning (EEW), which is an effective way for the earthquake emergency preparedness and earthquake disaster reduction, relies on the capability of rapidly detection of the first arrival wave (P-wave) and the accurate estimation of broadband displacements [1, 2]. Traditionally, EEW depends on seismic instruments [3–5], because broadband seismometers and strong-motion accelerometers measure velocity and acceleration with great accuracy, making them particularly effective at detecting ground motions [6]. The problem with seismic instruments is that they are prone to saturation, rotation and tilt during large earthquakes, and hence the earthquake-induced displacements through single integration or double integration of the observed waveforms are not reliable in real-time [7], which leads to underestimation of the earthquake's true size in the initial hours, such as the Sumatra earthquake [8] and the Tohoku-Oki earthquake [9]. Real-time high-rate GNSS, unlike seismic instruments, directly capture surface displacements at the sub-centimeter level with regard to an international terrestrial reference frame, meaning that they could provide reliable estimates of displacements during large magnitude events [1, 8]. However, due to the large high-frequency noise and the low sampling rates of GNSS measurements, it is hard to pick up the arrival time of P-wave accurately in GNSS-derived displacement history [10]. The complementary character of GNSS and seismic sensors are well recognized and the combination of them can be mutually beneficial in both sensitivity and large dynamic displacements [11].

In this study, we first introduce a new approach, namely the temporal point positioning (TPP) method, which could directly obtain coseismic (static and dynamic) displacements in real-time with a single GNSS receiver, then we apply a multi-rate Kalman filter to fuse GNSS-derived coseismic displacement with collocated accelerometer data for attaining displacements with a high precision and reliability, and further we detect the arrival time of P-wave, locate the epicenter and determine the magnitude. Finally, the performance of collocated GNSS and accelerometers was validated by using data from GEONET (1 Hz GPS) and K-NET/KiK-Net (100 Hz accelerometer) stations, with the collocated distance less

than 2 km, in the near field of the Mw 9.0 Tohoku-Oki earthquake occurred on March 11, 2011.

## 36.2 Estimation of GNSS Displacements Based on a Single Receiver

In the seismological applications, the displacement (position variation) of one station due to an earthquake is more curial information for EEW and source inversion. Currently, there are two strategies for a single GNSS receiver to obtain displacements between two appointed epochs. One strategy is that absolute position series are firstly calculated based on PPP [12], and then the displacement is obtained by subtracting one epoch position from the other epoch position [1, 11, 13–16]. The weakness of this approach is a long convergence period of ambiguity fixing. The other strategy is that velocities are determined at first, and then integrated together from one epoch to another epoch [17, 18]. In contrast with PPP, the latter one no longer needs a long convergence period since ambiguities are eliminated using the time difference of phase observations. However, this strategy has to face a problem that the integration process from velocities to displacements leads to a serious accumulated drift as long as the velocities contain few biases.

A novel method, namely TPP, is developed by Li et al. [19] to directly estimate coseismic displacement of one epoch relative to the chosen epoch with known coordinates. The model can be expressed as [19],

$$B_{r,j}^s(t_0) + t_r(t_0) + T_r^s(t_0) = l_{r,j}^s(t_0) + \mathbf{u}_r^s(t_0) \cdot x(t_0) + o^s(t_0) + t^s(t_0) + I_{r,j}^s(t_0) - \varepsilon_{r,j}^s(t_0) \quad (36.1)$$

$$\mathbf{u}_r^s(t_n) \cdot x(t_n) - t_r(t_n) - T_r^s(t_n) = -l_{r,j}^s(t_n) - t^s(t_n) - o^s(t_n) + B_{r,j}^s(t_n) - I_{r,j}^s(t_n) + \varepsilon_{r,j}^s(t_n) \quad (36.2)$$

$$B_{r,j}^s(t_n) = B_{r,j}^s(t_0) \quad (36.3)$$

$$\mathbf{u}_r^s(t_n) \cdot x(t_n) - \Delta t_r(t_0, t_n) = \mathbf{u}_r^s(t_0) \cdot x(t_0) - \Delta l_{r,j}^s(t_0, t_n) - \Delta t^s(t_0, t_n) - \Delta o^s(t_0, t_n) - \Delta I_{r,j}^s(t_0, t_n) + \Delta T_{r,j}^s(t_0, t_n) + \Delta \varepsilon_{r,j}^s(t_0, t_n) \quad (36.4)$$

where,  $s$  stands for a satellite,  $r$  stands for the GPS receiver,  $j$  stands for the frequency of L1 or L2 carrier phase,  $l_{r,j}^s$  is “observed minus computed” phase observations;  $\mathbf{u}_r^s$  is the receiver-to-satellite unit direction vector;  $x$  denotes receiver position;  $o^s$  denotes satellite orbit error;  $T_r^s, I_{r,j}^s$ , denote tropospheric and

ionospheric delay;  $t^s, t_r$  are satellite and receiver clock errors;  $B_{r,j}^s$  is the real-valued phase ambiguity;  $\varepsilon_{r,j}^s$  are measurement noise of carrier phase.

Equation (36.4) is final model of TPP, which is deduced from Eqs. (36.1) to (36.3). From the view of positioning, the core of the TPP model is that the estimated ambiguities  $B_{r,j}^s$  is fixed from the epoch  $t_0$  to  $t_n$ , and the well-known receiver position  $x(t_0)$  could be determined before the earthquake. With the satellite ephemeris and a certain prior models aided, all errors in Eq. (36.4) are corrected. Therefore, the receiver position  $x(t_n)$  can be accurately resolved and the associated displacement is obtained. From the view of position variation (displacement), Eq. (36.4) is in the same form as the time-differenced equation of phase observations under the condition that there are no cycle slips in observation data. After all errors corrected, the displacement of an arbitrary epoch  $t_n$  with respect to the chosen epoch  $t_0$  could be directly retrieved, which avoids the integration process of the Variometric approach described in Colosimo et al. [17]. Worth noting that different from the Variometric approach, the TPP method is based on the known accurate position at the chosen epoch, which is an important factor for achieving high-accuracy displacements [19].

### 36.3 Integrated Displacements Using a Kalman Filter

In order to estimate very high-rate accurate and reliable displacements in real time, a multi-rate Kalman filter to fuse GNSS-derived coseismic displacement with collocated accelerometer data is applied [10, 20].

In the integrated procedure, the discrete state equation can be expressed as [10],

$$x_k = \Phi_{k,k-1}x_{k-1} + B_{k,k-1}a_{k-1} + w_k \quad w_k \sim N(0, Q_{w_k}) \quad (36.5)$$

$$\Phi_{k,k-1} = \begin{bmatrix} 1 & \tau \\ 0 & 1 \end{bmatrix} \quad B_{k,k-1} = \begin{bmatrix} \tau^2/2 \\ \tau \end{bmatrix}$$

where  $x_k = [d_k \quad v_k]^T$  represents the state vector,  $\Phi_{k,k-1}$  is a transition matrix,  $B_{k, k-1}$  is an input matrix,  $\tau$  is the sampling interval of accelerometer.  $a_{k-1}$  is the raw accelerometer data as the system inputs.  $w_k$  is the state noise with the covariance matrix  $Q_{w_k}$ , which can be expressed as a function of Kalman filter process noise,

$$Q_{w_k} = \begin{bmatrix} \tau^3/3 \cdot \sigma_a^2 & \tau^2/2 \cdot \sigma_a^2 \\ \tau^2/2 \cdot \sigma_a^2 & \tau \cdot \sigma_a^2 \end{bmatrix} \quad (36.6)$$

where  $\sigma_a^2$  is the acceleration variance as a system dynamic noise.

The observational equation for the Kalman filter can be written as

$$l_k = A_k x_k + e_k \quad e_k \sim N(0, R_{e_k}) \quad (36.7)$$

$$R_{e_k} = \frac{r}{\tau_{GNSS}}$$

where  $l_k$  represents the observation (here is the GNSS displacement),  $A_k = [1 \ 0]^T$  is the design matrix, and  $e_k$  is the observation noise with  $R_{e_k}$  as its covariance matrix. The value of  $R_{e_k}$  is  $r/\tau_{GNSS}$ ,  $r$  denotes the GNSS displacement noise, and  $\tau_{GNSS}$  is the GNSS sampling interval.

The integrated results can be solved by the time update of Eq. (36.5) and the measurement update of Eq. (36.7) through a standard Kalman filter. It is noted that the time update is executed at every accelerometer sampling, and the measurement update with GNSS displacement is applied at every GNSS epoch.

## 36.4 Application to the 2011 Mw 9.0 Tohoku-Oki Earthquake

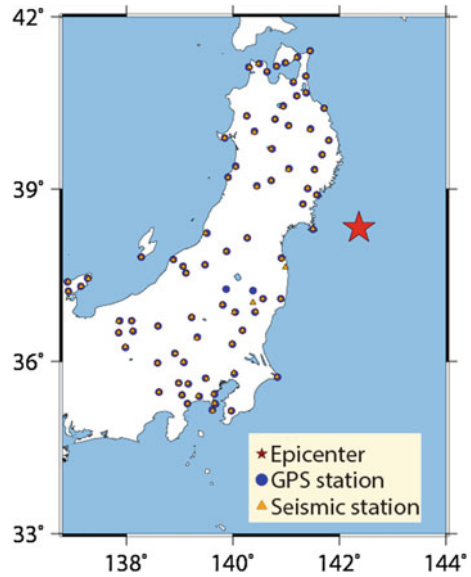
The Tohoku-Oki earthquake, occurred at 05:46:39 GPST on 11 March, 2011 in Japan with the moment magnitude 9.0, are well recorded by both accelerometer stations and high-rate GPS receivers. Following we will use the data to evaluate the performance of integrated displacements derived by the proposed method above.

Figure 36.1 shows a map of collocated GPS and accelerometer stations in the near-field areas within about 500 km from the epicenter (38.322°N, 142.369°E) as determined by the U. S. Geological Survey (abbr. USGS). GPS and accelerometer station pairs are chosen with distance less than 2 km of each other, which are considered effectively collocated [21]. GPS data are collected from GEONET stations with 1 Hz sample rate, and 100 Hz accelerometer data of K-Net and KiK-Net stations are provided by NIED.

### 36.4.1 TPP Analysis Using Only GPS Data

To evaluate the accuracy of the TPP method, we firstly processed all the GPS data collected at about 80 collocated stations before the earthquake. The results were converted to North/East/Up component and were compared with the zero displacement of truth. The TPP displacements of station 0550 for 15 min interval from 05:20:00 to 05:35:00 (GPST) are shown in Fig. 36.2. The red lines are the results, with consideration of three main error components mentioned in Sect. 36.2, using precise ephemeris, the ionosphere-free linear combination observation and the

**Fig. 36.1** Location of epicenter of the Tohoku-Oki earthquake ( $38.322^{\circ}\text{N}$ ,  $142.369^{\circ}\text{E}$ ) and the distribution map of collocated GPS and accelerometer stations. The *red star* stands for the epicenter. The *blue circles* stand for GPS sites. The *dark yellow triangles* represent accelerometer sites



accurate initial coordinates (PPP\_POPC\_LC solution). Meanwhile, we draw other displacements with different processing strategies to reflect the impact of those errors on TPP displacements. The blue line shows the results using precise ephemeris, the ionosphere-free linear combination observation and the coordinates derived from the standard position positioning (SPP) with 0.7 m error for North,  $-0.1$  m error for East, and 3.0 m error for Up component (SPP\_POPC\_LC solution). The black lines show the displacements using broadcast ephemeris, the ionosphere-free linear combination observation and the SPP-derived initial position (SPP\_BOBC\_LC solution). The results in cyan line are obtained by using broadcast ephemeris, the L1 carrier phase measurement and the SPP-derived initial position (SPP\_BOBC\_L1 solution).

From Fig. 36.2, the PPP\_POPC\_LC solution is close with the zero truth line with no obvious drift. After 15 min, the displacements are merely  $-1.0$ ,  $-0.6$ , and 2.5 cm for north/east/up components, respectively. Compared with the PPP\_POPC\_LC solution, the SPP\_POPC\_LC solution has a visible drift, and the drift values for 15 min are 6.6, 22.0, and 18.3 cm in north/east/up component. The SPP\_BOBC\_LC solution becomes more fluctuant with long-term variations due to the imprecise satellite orbit and clock correction, and the biases are several decimetres in the horizontal and vertical component. The ionospheric delay seems to be a big error source of TPP displacements, which could lead to about 1 m bias in the east and up component by comparison of the SPP\_BOBC\_LC solution and SPP\_BOBC\_L1 solution. From all four results, it is demonstrated that the PPP\_POPC\_LC solution is the most precise, which satisfies the demands of seismic monitoring and EEW. Considering that real-time precise orbit and precise clock corrections are available online via the IGS real-time pilot project, and the

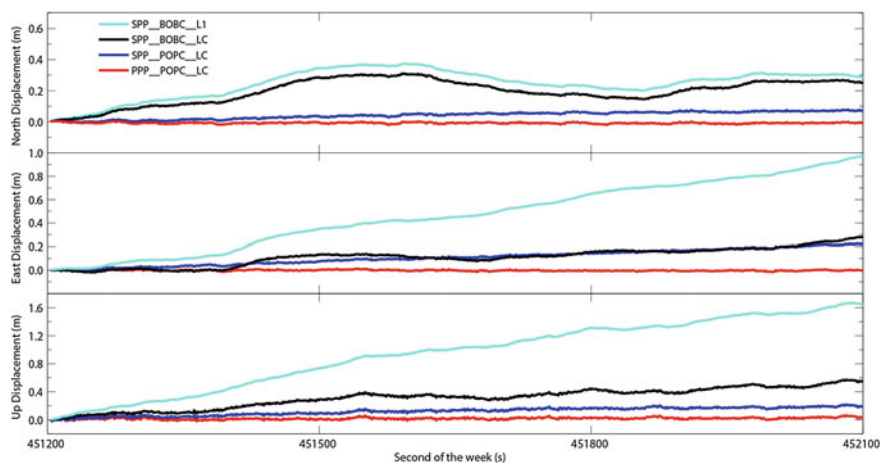


**Fig. 36.2** Displacements of station 0550 (38.3012°N, 141.5009°E) derived from TPP method. From *top to bottom* are the results in North/East/Up components

**Table 36.1** Root mean squares of the drift errors at about 80 sites

RMS (min)	North (cm)	East (cm)	Up (cm)
15	1.05	0.84	1.92
10	0.92	1.02	1.67
5	0.89	0.78	2.08
3	0.78	0.88	1.75
1	0.68	0.39	1.53

accurate site coordinates is usually well known, and thus the PPP\_POPC\_LC solution is accessible in real time during an earthquake. Here, we mainly focus on the PPP\_POPC\_LC solution in this study.

For the static period, TPP-derived displacements of all 80 sites at one certain epoch are compared with zero to calculate the root mean squares (RMS) as an indication of the TPP displacement accuracy. We respectively calculate the RMS values at different duration time (1, 3, 5, 10 and 15 min). The results are summarized in Table 36.1. The RMSs of the PPP\_POPC\_LC solution are stable from 1 to 15 min, and the values in north and east are almost within 1 cm, and in up with 2 cm, which is comparable to the accuracy of PPP after convergence period.

### 36.4.2 Integrated Displacements Analysis

In order to assess the performance of the integrated displacements, we compare them with GPS-only results derived from TPP and seismic-only waveforms derived from double integration of uncorrected acceleration data. As an example,

the nearest station pair is selected, which is K-NET station MYG011 (38.3052°N, 141.5044°E) and the GEONET station 0550 (38.3012°N, 141.5009°E), being separated by 560 m and located 75.7 km from the epicentre of the Tohoku-Oki earthquake. We adopt the approach stated in Sect. 39.3 to combine raw 100 Hz accelerations with 1 Hz TPP-derived displacements. The GPS displacement error is set to 1.0 cm for north/east and 2.0 cm for up component based on the above statistical RMS values. The acceleration noise is determined from windows (2–3 s) of pre-event accelerometer data or introduced from the empirical value, such as the K-NET acceleration precision is  $0.015 \text{ cm/s}^2$  [21]. Trifunac and Todorovska [22] demonstrated the rotation and tilt of accelerometer is a main source of acceleration noise during shaking, and thus we enlarge the pre-event acceleration noise by 1,000 times when the acceleration record value exceeds a certain times of the pre-event acceleration precision [10]. In addition, the acceleration changes rapidly during a large earthquake, and sometimes the change value in the sample interval (such as 0.01 s) could reach to several  $\text{cm/s}^2$  [23]. In such case, the system dynamics variance should be adjusted larger to fit the rapid state change.

Figure 36.3 shows the comparison of the integrated displacements and GPS-only/seismic-only displacements for the collocated stations MYG011/0550, and three sub-figures depict displacements for north/east/up components from the left to right. The uncorrected seismic displacements trace out the dynamic motions, but the latter portion of displacements drifts with a linear or parabolic trend. GPS-only solution is not drift in the displacement history and clearly depicts peak displacements and permanent offsets, which is demonstrated that the GPS-only displacements are good at low frequency band. However, the discrepancy of GPS-only displacement from the integrated displacements depicts a high-frequency noise of GPS-only results because of the low precision of GPS.

Compared to the GPS-only solution, the integrated displacements are remarkably improved by acceleration data in aspect of dynamical displacement precision, which can be used to detect P-wave arrival. We adopt the STA/LTA ratio method to automatically locate the arrival time of P-wave just as the same as done by Li et al. [2]. The window length of STA is 0.2 s, the window length of LTA is 2 s, and meanwhile the threshold of STA/LTA ratio is 10. As an example, Fig. 36.4 shows the first 20 s of the integrated results for station MYG011/0550 in up component and its corresponding STA/LTA ratio values. It is clearly shown that the STA/LTA ratio dramatically increases over the pre-set threshold when P-wave appears, and the detected arrival time of P-wave is 14.08 s after the origin time. Meanwhile, we do the same procedure for other four collocated station pairs (MYG001/0172, MYG003/0914, IWT013/0169, FKS001/0038) with the distance away the epicenter less than 150 km to obtain the P-wave arrival time, and the detected results are 17.33, 18.80, 20.01, 21.23 s, respectively, with a mean value 0.15 s offset different from the theoretical P-wave travel times calculated by TauP Toolkit.



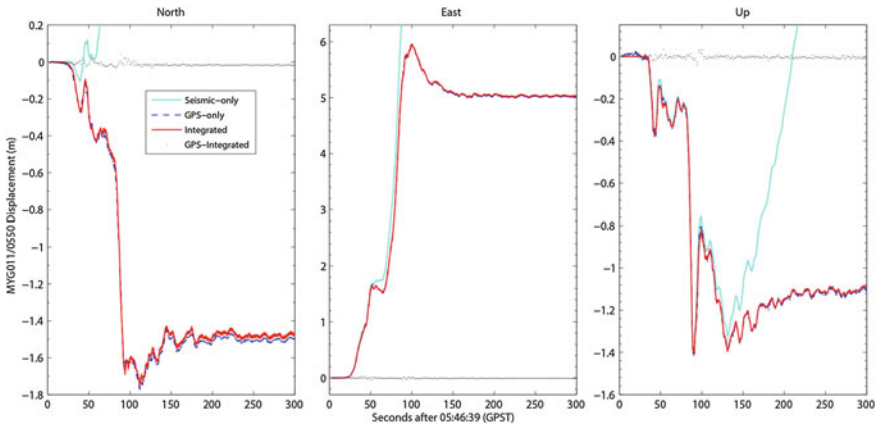


**Fig. 36.3** Comparison of seismic-only, GPS-only, and integrated displacements on the collocated MYG011 and 0550 stations for 300 s from the origin of the Tohoku-Oki earthquake. The red line depicts the integrated displacement (100 Hz), the cyan line depicts the uncorrected seismic-only displacement (100 Hz), the blue dotted line depicts the GPS-only displacement (1 Hz), and the black dots depict the discrepancy between integrated displacements and GPS-only displacements

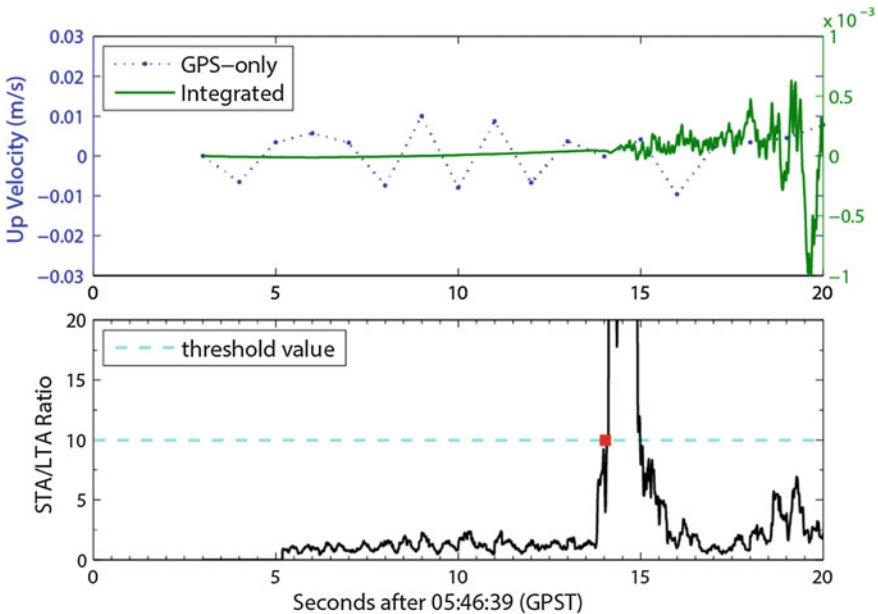


**Fig. 36.4** The first 20 s of the integrated velocities in up component on the collocated MYG011/0550 stations pair from the origin time of the Tohoku-Oki earthquake. The green line shows the integrated velocities (100 Hz), and the blue dotted line shows the GPS-only velocities (1 Hz). The black line in the bottom sub-figure is STA/LTA ratio results calculated from integrated velocities, and the red square point denotes the first arrival time of P-wave

### 36.4.3 *Magnitude Determination Through Attenuation Relationships of Peak Broadband Displacement*

For the issuing of effective tsunami warnings and emergency response, the rapid and accurate determination of the earthquake magnitude soon after a great earthquake is necessary. In order to rapidly determine the magnitude of impending earthquakes, several magnitude estimation methods based on P-wave have been developed [4, 24], which are effective for relatively small earthquakes. But for large earthquakes, they are problematic due to saturation effects [6]. To avoid the saturation problem, moment magnitude is applied for large earthquake magnitudes. However, moment magnitude, based on slip distribution inverted, is difficult to estimate in real time [25]. Taking into account the above-mentioned considerations, here we adopt the empirical scaling relationship between magnitude and peak ground displacement (PGD) to estimate the magnitude, which is deduced by Crowell et al. [26]. The scaling relationship is expressed as a function of moment magnitude  $M_w$  and hypocentral distance  $R$ ,

$$\log_{10}(PGD) = -5.013 + 1.219M_w - 0.178 \cdot \log_{10}(R) \quad (36.8)$$

We apply Eq. (36.8) to estimate the expected moment magnitude based on the integrated displacement results at every accelerometer sampling. Figure 36.5 shows the magnitude estimates as a function of time after earthquake origin for three collocated stations pairs. The pair MYG011/0550 station is the nearest from the earthquake source (source depth is defined as 29 km), the pair FKS013/0211 is located about 211 km from the source, and another pair KNG011/3065 is about 416.2 km. For the pair MYG011/0550 station, the estimated magnitude becomes stable at 115 s after the origin time of the earthquake, with a value of  $M_w$  8.88. For the pair FKS013/0211 station, the final estimated magnitude is  $M_w$  9.12 at 145 s. And the magnitude determined by the pair KNG011/3065 station could reach  $M_w$  9.16 at 196 s. It is demonstrated that the moment magnitude can be correctly determined within 2–3 min after earthquake initiation. In Fig. 36.6, the recorded peak displacements distribute around the reference line, indicating that the attenuation in log of peak displacement is proportional to log of hypocentral distance. The magnitude estimates from all 80 collocated stations are well within the uncertainties of the scaling relationship (the uncertainty is 0.224 demonstrated in Crowell et al. [26]), with a mean magnitude value is 9.06. It is shown that a reliable magnitude is achievable within 2–3 min using a few near-field collocated stations.

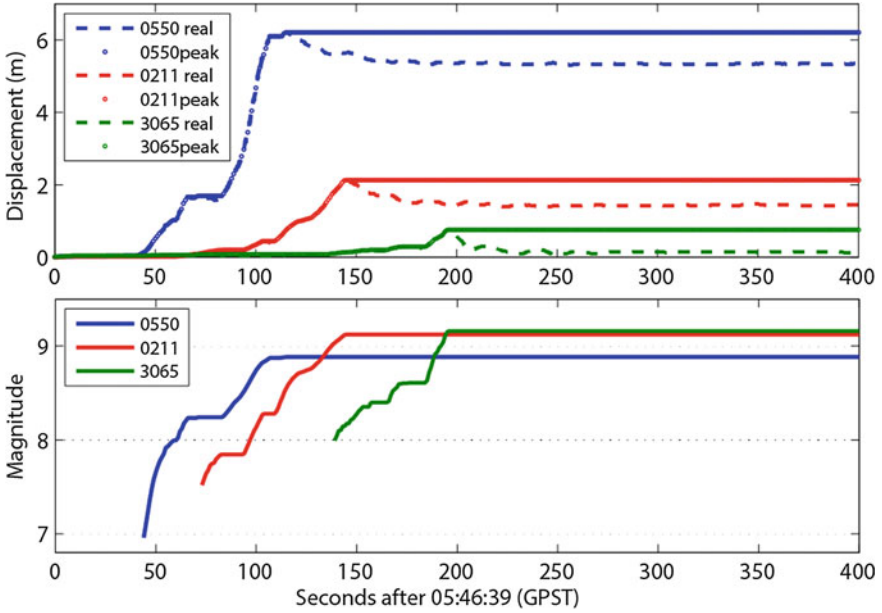


**Fig. 36.5** Magnitude estimates after earthquake origin for the Tohoku-Oki earthquake. The *top* sub-figure is the 3D displacement waveform for three collocated stations pairs MYG011/0550 (*blue*), FKS013/0211 (*red*), and KNG011/3065 (*green*). The *solid line* represents the real displacement, and the *dot line* denotes the peak displacement up to the current

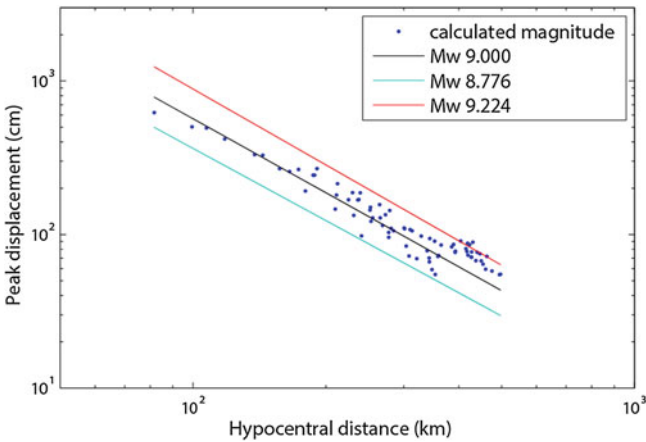


**Fig. 36.6** Relation between peak 3D displacement and hypocentral distance. The *black line* represents the reference value (Mw 9.0) calculated by Eq. (36.8) with one standard deviation of 0.224 in *red line* (Mw 9.224) and *cyan line* (Mw 8.776). The recorded displacements of collocated stations (*blue dots*) scatter around the expected line of Mw 9.0

## 36.5 Conclusions

This study investigates the joint use of the collocated GNSS and acceleration data for earthquake early warning. The performance was validated based on the collocated GPS and acceleration data collected during the 2011 Tohoku-Oki earthquake, and here comes some conclusion as follows,

- (1) The TPP method is a quite suitable way for obtaining coseismic displacement with a single GNSS receiver in real-time, which overcomes the convergence problem of PPP and avoids the integration process for the velocity estimation approach.
- (2) The accuracy of TPP solution by using the precise satellite ephemeris, the ionosphere-free linear combination observation and the accurate initial coordinates are 1 cm in north and east component, and 2 cm in up component during a few to tens of minutes.
- (3) A more accurate and reliable broadband displacement could be obtained by a multi-rate Kalman filter, which provides the full spectrum of the seismic motion. It is noteworthy that the acceleration noise as a system process noise should be adjusted larger to fit the rapid state change with consideration of the station dynamic status during shaking period.
- (4) Based on the broadband displacements, the arrival time of P-wave can be picked up accurately with a mean value 0.15 s offset, and the magnitude for large earthquake could be estimated robustly and rapidly. For the Tohoku-Oki earthquake, the estimated magnitude is Mw 9.06, which can be determined within 2–3 min after earthquake initiation.

**Acknowledgments** The K-NET and KiK-Net strong-motion data for the 2011 Tohoku earthquake were provided by the National Research Institute for Earth Science and Disaster Prevention (NIED) of Japan. GEONET (GPS Earth Observation Network System) data was provided by the Geospatial Information Authority of Japan (GSI). Thanks also to the International GNSS Service (IGS) for providing GPS data of globally distributed reference stations. This study was supported by Specialized Research Fund for the Doctoral Program of Higher Education of China (Grant No. 20130141110001), National Natural Science Foundation of China (Grant No. 41074024, No. 41204030), National 973 Project China (Grant No. 2013CB733301), the Fundamental Research Funds for the Central Universities (No.: 2012214020207) and the Surveying and Mapping Foundation Research Fund Program, National Administration of Surveying, Mapping and Geoinformation (12-02-010).

## References

1. Allen RM, Ziv A (2011) Application of real-time GPS to earthquake early warning. *Geophys Res Lett* 38:L16310
2. Li X, Zhang X, Guo B (2013) Application of collocated GPS and seismic sensors to earthquake monitoring and early warning. *Sensors* 13:14261–14276

3. Aranda JE, Jimenez A, Ibarrola G, Alcantar F, Aguilar A, Inostroza M, Maldonado S (1995) Mexico City seismic alert system. *Seismol Res Lett* 66:42–53
4. Allen RM, Kanamori H (2003) The potential for earthquake early warning in southern California. *Science* 300:786–789
5. Kanamori H (2007) Real-time earthquake damage mitigation measures. In: Gasparini P, Manfredi G, Zschau J (eds) *Earthquake early warning systems*. Springer, Berlin, Heidelberg
6. Allen RM, Gasparini P, Kamigaichi O, Bose M (2009) The status of earthquake early warning around the world: an introductory overview. *Seismol Res Lett* 80:682–693
7. Wang R, Schurr B, Milkereit C, Shao Z, Jin M (2011) An improved automatic scheme for empirical baseline correction of digital strong-motion records. *B Seismol Soc Am* 101:2029–2044
8. Blewitt G, Kreemer C, Hammond WC, Plag HP, Stein S, Okal E (2006) Rapid determination of earthquake magnitude using GPS for tsunami warning systems. *Geophys Res Lett* 33:L11309
9. Ohta Y, Kobayashi T, Tsushima H, Miura S, Hino R, Takasu T, Fujimoto H, Inuma T, Tachibana K, Demachi T, Sato T, Ohzono M, Umino N (2012) Quasi real-time fault model estimation for near-field tsunami forecasting based on RTK-GPS analysis: application to the 2011 Tohoku-Oki earthquake (Mw 9.0). *J Geophys Res* 117:B2311
10. Bock Y, Melgar D, Crowell BW (2011) Real-time strong-motion broadband displacements from collocated GPS and accelerometers. *B Seismol Soc Am* 101:2904–2925
11. Xu P, Shi C, Fang R, Liu J, Niu X, Zhang Q, Yanagidani T (2013) High-rate precise point positioning (PPP) to measure seismic wave motions: an experimental comparison of GPS PPP with inertial measurement units. *J Geodesy* 87:361–372
12. Zumberge JF, Hefflin MB, Jefferson DC, Watkins MM, Webb FH (1997) Precise point positioning for the efficient and robust analysis of GPS data from large networks. *J Geophys Res* 102:5005–5017
13. Kouba J (2003) Measuring seismic waves induced by large earthquakes with GPS. *Stud Geophys Geodesy* 47:741–755
14. Wright TJ, Houlie N, Hildyard M, Iwabuchi T (2012) Real-time, reliable magnitudes for large earthquakes from 1 Hz GPS precise point positioning: the 2011 Tohoku-Oki (Japan) earthquake. *Geophys Res Lett* 39:L12302
15. Li X, Ge M, Zhang X, Zhang Y, Guo B, Wang R, Klotz J, Wickert J (2013) Real-time high-rate coseismic displacement from ambiguity-fixed precise point positioning: application to earthquake early warning. *Geophys Res Lett* 40:295–300
16. Geng J, Bock Y, Melgar D, Crowell BW, Haase JS, Cecil H, Ida M (2013) A new seismogeodetic approach applied to GPS and accelerometer observations of the 2012 Brawley seismic swarm: implications for earthquake early warning. *Geochem Geophys Geosyst* 14:2124–2142
17. Colosimo G, Crespi M, Mazzoni A (2011) Real-time GPS seismology with a stand-alone receiver: a preliminary feasibility demonstration. *J Geophys Res* 116:B11302
18. Zhang X, Guo B (2013) Real-time tracking the instantaneous movement of crust during earthquake with a stand-alone GPS receiver. *Chin J Geophys* 56:1928–1936 (in Chinese)
19. Li X, Ge M, Guo B, Wickert J, Schuh H (2013) Temporal point positioning approach for real-time GNSS seismology using a single receiver. *Geophys Res Lett* 40:5677–5682
20. Smyth A, Wu M (2007) Multi-rate Kalman filtering for the data fusion of displacement and acceleration response measurements in dynamic system monitoring. *Mech Syst Signal Process* 21:706–723
21. Emore GL, Haase JS, Choi K, Larson KM, Yamagiwa A (2007) Recovering seismic displacements through combined use of 1-Hz GPS and strong-motion accelerometers. *B Seismol Soc Am* 97:357–378
22. Trifunac MD, Todorovska MI (2001) A note on the usable dynamic range of accelerographs recording translation. *Soil Dyn Earthq Eng* 21:275–286

23. Tu R, Ge M, Wang R, Walter TR (2014) A new algorithm for tight integration of real-time GPS and strong-motion records, demonstrated on simulated, experimental, and real seismic data. *J Seismol* 18:151–161
24. Kanamori H (2005) Real-time seismology and earthquake damage mitigation. *Annu Rev Earth Planet Sci* 33:195–214
25. Fang R, Shi C, Song W, Wang G, Liu J (2013) Determination of earthquake magnitude using GPS displacement waveforms from real-time precise point positioning. *Geophys J Int*. doi:[10.1093/gji/ggt378](https://doi.org/10.1093/gji/ggt378)
26. Crowell BW, Melgar D, Bock Y, Haase JS, Geng J (2013) Earthquake magnitude scaling using seismogeodetic data. *Geophys Res Lett* 40:6089–6094